Journal of Computational Science and Technology

Vol. 2, No. 4, 2008

Constitutive Modeling of Porous Shape Memory Alloys Considering Strain Rate Effect*

Yutaka TOI** and Daegon CHOI**

**Institute of Industrial Science, University of Tokyo

4-6-1 Komaba, Meguro-ku, Tokyo, Japan

E-mail:toi@iis.u-tokyo.ac.jp

Abstract

The existing one-dimensional constitutive model for shape memory alloys is extended to take account of the porosity and the strain rate effect by using the internal state variables representing the porosity and the martensite volume fraction. The proposed constitutive equation is applied to the simulations for the quasi-static and the dynamic behaviors of dense and porous shape memory alloys at various temperatures and strain rates. The calculated results are compared with the uniaxial test results for dense and porous NiTi alloys to illustrate the validity of the present constitutive modeling. It is expected that the finite element program implementing the proposed constitutive equation will be a powerful tool to predict the mechanical behaviors of various porous shape memory alloy devices.

Key words: Computational Mechanics, Structural Analysis, Constitutive Modeling, Strain Rate, Porous Shape Memory Alloy, Superelasticity

1. Introduction

Intelligent materials are promising in the research and development of new materials of the 21st century as they are soft, reliable and resource/energy-saving. Shape memory alloys (abbreviated as SMAs) have been applied to various practical devices as the materials with actuating and sensing functions. The SMAs are applicable to the aeronautical and the medical engineering field because of their light weight and biocompatibility[1]. The shape memory effect and the superelasticity of the SMAs are widely utilized in these applications, while the high energy absorbing capability of the SMAs has little been studied.

The porous shape memory alloys (abbreviated as PSMAs), which have a high specific damping capability under dynamic loading, can be formed into porosity-graded materials[2]. The computational prediction of the mechanical behaviors of the PSMAs is required for the efficient and optimal design and development of the PSMA devices. The formulations by the micromechanics-based approach given by Nemat-Nasser et al.[3] and Entchev et al.[4] are known as the constitutive equations for the PSMAs.

The present study is based on the macroscopic, phenomenological one-dimensional constitutive equation for the SMAs given by the authors[5], which is extended to the constitutive model considering the porosity and the strain-rate effect. The calculated results are compared with the experimental results given by Zhao et al.[1] and Nemat-Nasser[3),(6] to illustrate the validity of the present constitutive equation model.

The section 2 describes the formulation of the constitutive equation for the PSMAs. The calculated results for the quasi-static and the dynamic behaviors of the dense SMAs and the PSMAs are compared with the experimental results in the section 3. The section 4 contains the concluding remarks.

*Received 7 Oct., 2008 (No. T1-06-1257)
Japanese Original : Trans. Jpn. Soc. Mech. Eng., Vol.73, No.731, A (2007), pp.753-760 (Received 28 Dec., 2006)
[DOI: 10.1299/jcst.2.511]

2. Constitutive Equation for Porous Shape Memory Alloys

2.1 Quasi-Static Constitutive Equation

The mechanical characteristic of the SMAs to be discussed in the present study is schematically shown in Fig. 1. Figure 1(a) shows the superelastic behavior (bold line arrows) and the shape memory effect (dotted line arrows), while Fig. 1(b) shows the relation between the critical transformation stresses and the temperature. In Fig. 1, the following notations are used: σ; the stress, ε; the strain, T; the temperature, σ_f^{cr} and σ_s^{cr}; the critical stress for finishing and starting martensite transformation, C_M and C_A; the gradient of the critical transformation stresses with respect to the temperature, M_f and M_s; the critical temperature for finishing and starting martensite transformation, A_s and A_f; the critical temperature for starting and finishing austenite transformation. The stress loading and unloading at the temperature higher than A_f as indicated in Fig. 1(b) causes the superelastic behavior as shown in Fig. 1(a).

The one-dimensional stress-strain relation for the SMAs is generally expressed by the following equation:

$$\sigma = E \cdot \varepsilon + \Omega \cdot \xi_s + \theta \cdot T \tag{1}$$

where ξ_S, E, Ω and θ are the stress-induced martensite volume fraction, Young's modulus, the transformation coefficient and the thermal elastic constant, respectively. The subscript '0' indicates the initial value.

Using the maximum residual strain ε_L, the transformation constant Ω is expressed as follows:

$$\Omega = -\varepsilon_L E \tag{2}$$

Young's modulus E is expressed in terms of the martensite volume fraction ξ as follows:

$$E = E_a + \xi(E_m - E_a) \tag{3}$$

where E_m and E_a are Young's modulus of the martensite phase and the austenite phase, respectively. Using the temperature induced martensite volume fraction ξ_T, the total martensite volume fraction is expressed as

$$\xi = \xi_S + \xi_T \tag{4}$$

ξ, ξ_S and ξ_T are the functions of the temperature T and the stress σ.

Drucker-Prager equivalent stress is expressed as

$$\sigma^{DP} = \sigma_e + 3\beta p \tag{5}$$

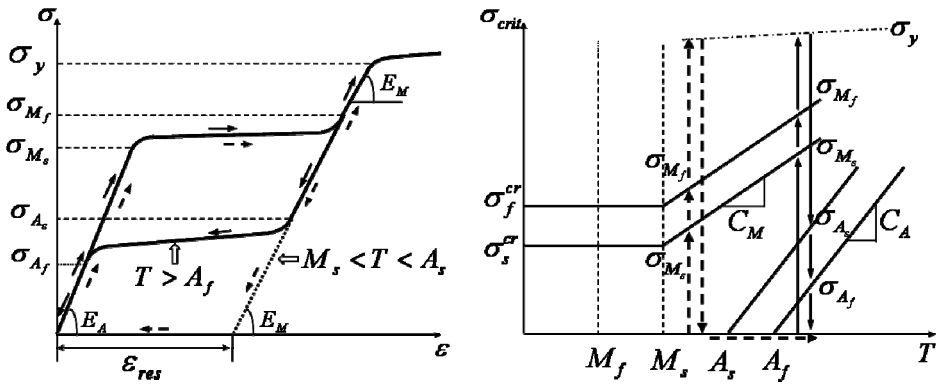

(a) Superelastic behavior and shape memory effect

(b) Critical stresses for transformations vs. temperature

Fig. 1 Mechanical properties of shape memory alloys

where σ_e and β are von Mises equivalent stress and a material constant, respectively. p is the hydrostatic pressure given by the following equation:

$$p = \frac{1}{3}\left(\sigma_x + \sigma_y + \sigma_z\right) \tag{6}$$

β=0.15 given by Auricchio and Taylor[7] is assumed in the present calculations. The present study discusses only the uniaxial stress state. Assuming that the superelastic behavior of the PSMAs is governed only by the uniaxial normal stress σ_z, the equivalent stress is defined by the following equation:

$$\sigma^{DP} = \left|\sigma_z\right| + 3\beta\sigma_z \tag{7}$$

The porosity f as follows is used according to Zhao et al.[1] in order to take account of the effect of porosity:

$$0 \le f \le 1 \tag{8}$$

Considering the porosity, Young's modulus, the transformation constant and Drucker-Prager equivalent stress are expressed as follows:

$$\overline{E} = E\left(1 - \eta_E f\right) \tag{9}$$

$$\overline{\Omega} = -\varepsilon_L \overline{E} = -\varepsilon_L E\left(1 - \eta_E f\right) \tag{10}$$

$$\overline{\sigma}^{DP} = \frac{\sigma^{DP}}{1-f} = \frac{\left|\sigma_z\right| + 3\beta\sigma_z}{1-f} \tag{11}$$

where η_E is a material constant. The upper bar ($\overline{\ }$) indicates the variables considering the porosity. In the present calculations, η_E=3 is used referring to Toi and Kiyosue[8]. Equation (1) can be rewritten as follows:

$$\sigma = \overline{E}\cdot\varepsilon + \overline{\Omega}\cdot\xi_s + \theta\cdot T \tag{12}$$

Introducing Eq. (11) into the evolution equations[5] of ξ, ξ_S and ξ_T for the SMAs, the following evolution equations for the transformation processes to the martensite and the austenite phase can be obtained:

(i) Transformation process to the martensite phase

・In the case when $T > M_s$ and

$\sigma_s^{cr}(1+\beta) + C_M(1+\beta)(T - M_s) < \overline{\sigma}^{DP} < \sigma_f^{cr}(1+\beta) + C_M(1+\beta)(T - M_s)$

$$\xi_S = \frac{1-\xi_{S0}}{2}\cos\left\{\frac{\pi}{\left(\sigma_s^{cr} - \sigma_f^{cr}\right)}\left[\frac{\overline{\sigma}^{DP}}{(1+\beta)} - \sigma_f^{cr} - C_M\left(T - M_s\right)\right]\right\} + \frac{1+\xi_{S0}}{2} \tag{13}$$

$$\xi_T = \xi_{T0} - \frac{\xi_{T0}}{1-\xi_{S0}}\left(\xi_S - \xi_{S0}\right) \tag{14}$$

・In the case when $T < M_s$ and $\sigma_s^{cr}(1+\beta) < \overline{\sigma}^{DP} < \sigma_f^{cr}(1+\beta)$

$$\xi_S = \frac{1-\xi_{S0}}{2}\cos\left\{\frac{\pi}{\left(\sigma_s^{cr} - \sigma_f^{cr}\right)}\left[\frac{\overline{\sigma}^{DP}}{(1+\beta)} - \sigma_f^{cr}\right]\right\} + \frac{1+\xi_{S0}}{2} \tag{15}$$

$$\xi_T = \xi_{T0} - \frac{\xi_{T0}}{1-\xi_{S0}}\left(\xi_S - \xi_{S0}\right) + \Delta_{T\xi} \tag{16}$$

where, if $M_f < T < M_s$ and $T < T_0$

$$\Delta_{T\xi} = \frac{1-\xi_{T0}}{2}\left\{1 + \cos\left[a_M\left(T - M_f\right)\right]\right\} \tag{17}$$

else

$$\Delta_{T\xi} = 0 \tag{18}$$

(ii) Transformation process to the austenite phase

· In the case when $T > A_s$ and $C_A(1+\beta)(T-A_f) < \overline{\sigma}^{DP} < C_A(1+\beta)(T-A_s)$

$$\xi = \frac{\xi_0}{2}\left\{1+\cos\left[a_A\left(T-A_S-\frac{\overline{\sigma}^{DP}}{C_A(1+\beta)}\right)\right]\right\} \tag{19}$$

$$\xi_S = \xi_{S0} - \frac{\xi_{S0}}{\xi_0}(\xi_0 - \xi) \tag{20}$$

$$\xi_T = \xi_{T0} - \frac{\xi_{T0}}{\xi_0}(\xi_0 - \xi) \tag{21}$$

where a_M and a_A are defined by the following equations:

$$a_M = \frac{\pi}{M_s - M_f}, \quad a_A = \frac{\pi}{A_f - A_s} \tag{22}$$

2.2 Constitutive Equation Considering the Strain Rate Effect

The present subsection discusses the constitutive equation for the PSMAs considering the strain rate effect. The strain rate is defined as

$$\dot{\varepsilon} = \frac{\Delta\varepsilon}{\Delta t} \tag{23}$$

The following sign function is used:

$$sign(x) = \begin{cases} +1 & if\ x > 0 \\ 0 & if\ x = 0 \\ -1 & if\ x < 0 \end{cases} \tag{24}$$

The time differentiation of the general stress-strain relation (12) for the PSMAs leads to the following expression:

$$\dot{\sigma} = \dot{\overline{E}} \cdot \varepsilon + \overline{E} \cdot \dot{\varepsilon} + \dot{\overline{\Omega}} \cdot \xi_s + \overline{\Omega} \cdot \dot{\xi}_s + \theta \cdot \dot{T} \tag{25}$$

Differentiating Young's modulus (9) and the transformation coefficient (10) considering the porosity with respect to the time, the following equations can be obtained:

$$\dot{\overline{E}} = \dot{E}(1-\eta_E f) = \dot{\xi}(E_m - E_a)(1-\eta_E f) \tag{26}$$

$$\dot{\overline{\Omega}} = -\varepsilon_L \dot{\overline{E}} = -\varepsilon_L \dot{\xi}(E_m - E_a)(1-\eta_E f) \tag{27}$$

Applying Euler's formula for the numerical time integration to Eq. (25), it can be rewritten as

$$\begin{aligned} &\sigma_{n+1} - \sigma_n = \overline{E}_n \Delta\varepsilon_n \\ &+ \Delta t_n \left\{\dot{\overline{E}}_n \varepsilon_n + sign(\sigma_n)\overline{\Omega}_n \dot{\xi}_{S_n} + sign(\sigma_n)\dot{\overline{\Omega}}\xi_{S_n} + sign(\sigma_n)\Theta\dot{T}_n\right\} \end{aligned} \tag{28}$$

The evolution equations (13)-(22) for the transformation processes to the martensite and the austenite phase are extended as follows to take account of the strain rate effect. This extension formally follows the constitutive equation for brittle microcracking solids[9] considering the strain rate effect. The evolution equation for the time rate of the martensite volume fraction is mathematically similar to the viscoplastic flow rule[10].

(i) Transformation process to the martensite phase

・In the case of $T > M_s$

① $\bar{\sigma}^{DP} \le \sigma_s^{cr}(1+\beta) + C_M(1+\beta)(T - M_s)$:

$$\xi = 0 \tag{29}$$

$$\dot{\xi} = 0 \tag{30}$$

② $\xi < 1$ and $\bar{\sigma}^{DP} > \sigma_{MS1}(\xi)$:

$$\dot{\xi}_S = \frac{1}{\eta}\left\{\frac{\bar{\sigma}^{DP}}{\sigma_{MS1}(\xi_S)} - 1\right\}^{\gamma} \tag{31}$$

$$\dot{\xi} = \frac{1}{\eta}\left\{\frac{\bar{\sigma}^{DP}}{\sigma_{MS1}(\xi)} - 1\right\}^{\gamma} \tag{32}$$

where η and γ are the viscous coefficient and a material constant, respectively. $\sigma_{MS1}(\xi)$ and $\sigma_{MS1}(\xi_S)$ are defined by the following equations:

$$\sigma_{MS1}(\xi) = (1+\beta)\left[\sigma_f^{cr} + C_M(T - M_s) + \frac{(\sigma_s^{cr} - \sigma_f^{cr})}{\pi}\cos^{-1}\left(\frac{2\xi - \xi_0 - 1}{1 - \xi_0}\right)\right] \tag{33}$$

$$\sigma_{MS1}(\xi_S) = (1+\beta)\left[\sigma_f^{cr} + C_M(T - M_s) + \frac{(\sigma_s^{cr} - \sigma_f^{cr})}{\pi}\cos^{-1}\left(\frac{2\xi_S - \xi_{S0} - 1}{1 - \xi_{S0}}\right)\right] \tag{34}$$

③ $\xi \ge 1$:

$$\xi = 1 \tag{35}$$

$$\dot{\xi} = 0 \tag{36}$$

・In the case of $T < M_s$

① $\bar{\sigma}^{DP} \le \sigma_s^{cr}(1+\beta)$:

$$\xi = 0 \tag{29}$$

$$\dot{\xi} = 0 \tag{30}$$

② $\xi < 1$ and $\bar{\sigma}^{DP} > \sigma_{MS2}(\xi)$:

$$\dot{\xi}_S = \frac{1}{\eta}\left\{\frac{\bar{\sigma}^{DP}}{\sigma_{MS2}(\xi_S)} - 1\right\}^{\gamma} \tag{37}$$

$$\dot{\xi} = \frac{1}{\eta}\left\{\frac{\bar{\sigma}^{DP}}{\sigma_{MS2}(\xi)} - 1\right\}^{\gamma} \tag{38}$$

where $\sigma_{MS2}(\xi)$ and $\sigma_{MS2}(\xi_S)$ are defined by the following equations:

$$\sigma_{MS2}(\xi) = (1+\beta)\left[\sigma_f^{cr} + \frac{(\sigma_s^{cr} - \sigma_f^{cr})}{\pi}\cos^{-1}\left(\frac{2\xi - \xi_0 - 1 - 2\Delta_{T\xi}}{1 - \xi_0}\right)\right] \tag{39}$$

$$\sigma_{MS2}(\xi_S) = (1+\beta)\left[\sigma_f^{cr} + \frac{(\sigma_s^{cr} - \sigma_f^{cr})}{\pi}\cos^{-1}\left(\frac{2\xi_S - \xi_{S0} - 1}{1 - \xi_{S0}}\right)\right] \tag{40}$$

③ $\xi \ge 1$:

$$\xi = 1 \tag{35}$$

$$\dot{\xi} = 0 \tag{36}$$

(ii) Transformation process to the austenite phase

・In the case of $T > A_s$

① $\bar{\sigma}^{DP} \geq C_A(1+\beta)(T - A_s)$:

$$\xi = 1 \tag{29}$$

$$\dot{\xi} = 0 \tag{30}$$

② $\xi < 1$ and $\bar{\sigma}^{DP} < \sigma_{AS}(\xi)$:

$$\dot{\xi}_S = \frac{1}{\eta}\left\{\frac{\bar{\sigma}^{DP}}{\sigma_{AS}(\xi_S)} - 1\right\}^{\gamma} \tag{41}$$

$$\dot{\xi} = \frac{1}{\eta}\left\{\frac{\bar{\sigma}^{DP}}{\sigma_{AS}(\xi)} - 1\right\}^{\gamma} \tag{42}$$

where $\sigma_{AS}(\xi)$ and $\sigma_{AS}(\xi_S)$ are defined by the following equations:

$$\sigma_{AS}(\xi) = C_A(1+\beta)\left[T - A_S - \frac{1}{a_A}\cos^{-1}\left(\frac{2\xi}{\xi_0} - 1\right)\right] \tag{43}$$

$$\sigma_{AS}(\xi_S) = C_A(1+\beta)\left[T - A_S - \frac{1}{a_A}\cos^{-1}\left(\frac{2\xi_S}{\xi_{S0}} - 1\right)\right] \tag{44}$$

③ $\xi \leq 0$:

$$\xi = 0 \tag{35}$$

$$\dot{\xi} = 0 \tag{36}$$

The strain rate dependence of the SMAs at a high speed deformation is related to the increase of the critical stress for the martensite transformation caused by the temperature increase due to the latent heat and the heat generation accompanied by the deformation during the martensite transformation. The strain rate dependent constitutive equation derived in the present subsection is a phenomenological formulation, in which the material behavior at a high speed deformation including the increasing effect of the critical transformation stress is represented in the qualitatively similar mathematical form to the macroscopic theory of viscoplasticity. The increase in the number of the material constants is suppressed to the minimum. It is noted that the above-stated temperature increase is not considered in the temperature T in the formulation.

3. Computational Results

3.1 Static Behavior of the PSMAs

The calculated results for the static behaviors of the dense SMA(50.9Ni-49.1Ti(at.%)) and the 13% PSMA (50.9Ni-49.1Ti(at.%)) are compared with the experimental results given by Zhao et al.[1] in the present subsection. The temperature for the compressive calculations is 58℃ which is higher than the temperature for finishing austenite transformation (A_f).

Table 1 shows the material constants used in the calculations. The critical stresses for the martensite and the austenite transformation are shown in Table 2. The specimens have been deformed up to the strain of 0.0458. The minus sign in the table indicates a compressive stress. The calculated results for the two specimens are shown in Fig. 2 and Fig. 3, which are the stress-strain relation for the dense SMA and the 13% PSMA, respectively.

Table 1 Material constants of NiTi dense SMAs (50.9Ni-49.1Ti (at.%))

Modulus	E_a(MPa)	75000
	E_m(MPa)	53000
	θ (MPa/℃)	0.55
	β	0.15
Transformation temperatures	A_s(℃)	23.88
	A_f(℃)	43.12
	M_s(℃)	36.05
	M_f(℃)	23.09
Maximum residual strain	ε_L	0.023

Table 2 Critical transformation stresses

	Dense SMAs	Porous SMAs
σ_{Ms}(MPa)	-252	-187
σ_{Mf}(MPa)	-1212	-1161
σ_{As}(MPa)	-684	-465
σ_{Af}(MPa)	-95	-87

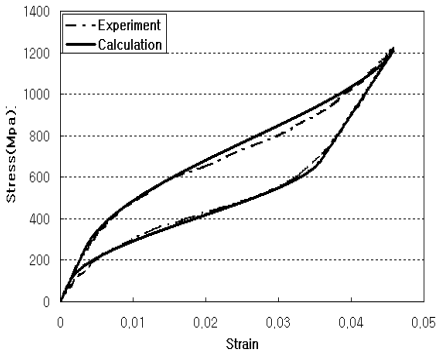

Fig. 2 Compressive stress-strain curves of dense SMAs at 58℃

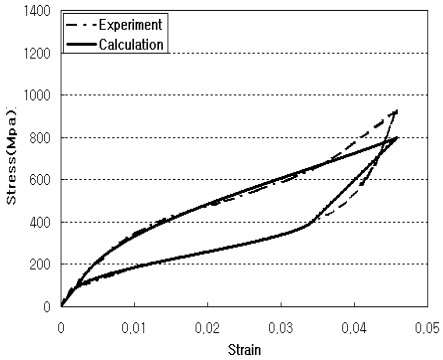

Fig. 3 Compressive stress-strain curves of 13% porosity SMAs at 58℃

The complete superelastic behavior takes place as the martensite transformation is induced by the stress and the inverse transformation is finished during the unloading process. The rigidity for the martensite phase immediately after the unloading is smaller than the rigidity for the austenite phase during the initial loading. The rigidity for the PSMA is smaller than that for the dense SMA.

It is seen that the present constitutive modeling for the PSMAs is valid as the static superelastic behaviors for the dense SMA and the 13% PSMA are totally well indentified by the present modeling.

3.2 Quasi-static and Dynamic Behaviors of the SMAs

The calculated results for the quasi-static and the dynamic behaviors of the dense SMA (50.4Ni-49.6Ti(at.%)) are compared with the experimental results given by Nemat-Nasser et al.[6] in the present subsection. The temperature is 23℃ which coincides with the temperature for finishing the austenite transformation (A_f).

The material constants used in the quasi-static calculations are shown in Table 3. Figure 4 shows the calculated results for the stress-strain relations of the dense SMAs at four relatively low strain rates (1/s, 10^{-1}/s, 10^{-2}/s, 10^{-4}/s), which are compared with the experimental results. It is observed in the experimental results that the strain hardening rate during the martensite transformation and the residual strain after the unloading depend on the strain rate. Although such phenomena are

qualitatively well simulated by the present constitutive equation model, there is a room for improvement for the shape of the stress-strain curves.

The material constants used in the dynamic calculations are shown in Table 4. Figure 5 shows the calculated results for the stress-strain relations of the dense SMAs at four relatively high strain rates (1080/s, 610/s, 570/s, 330/s), which are compared with the experimental results. Although the calculated results totally correspond well with the experimental results, the material constants identified for the high speed deformation (Table 4) slightly differ from those for the low speed deformation (Table 3). It is suggested that the material constants in the present constitutive equation model are still strain rate dependent.

Table 3 Material constants of NiTi dense SMAs for low strain rates (50.4Ni-49.6Ti (at.%))

Modulus	E_a(MPa)	35000
	E_m(MPa)	43000
	θ (MPa/℃)	0.55
	β	0.15
	η (sec)	0.15
	γ	4.0
Critical transformation stresses	σ_{Ms}(MPa)	-200
	σ_{Mf}(MPa)	-315
	σ_{As}(MPa)	9
	σ_{Af}(MPa)	32
Maximum residual strain	ε_L	0.052

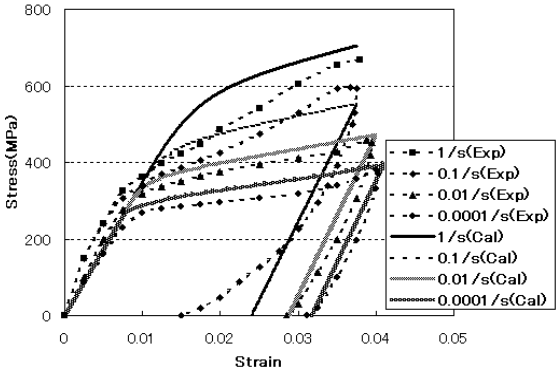

Fig. 4 Quasi-static stress-strain curves of dense SMAs at a constant temperature of 23℃ and the indicated strain rates

Table 4 Material constants of NiTi dense SMAs for high strain rates (50.4Ni-49.6Ti (at.%))

Modulus	E_a(MPa)	40000
	E_m(MPa)	50000
	θ(MPa/℃)	0.55
	β	0.15
	η (sec)	1.8×10^{-5}
	γ	1
Critical transformation stresses	σ_{Ms}(MPa)	-240
	σ_{Mf}(MPa)	-677
	σ_{As}(MPa)	-445
	σ_{Af}(MPa)	10
Maximum residual strain	ε_L	0.05

3.3 Quasi-static and Dynamic Behaviors of the PSMAs

The calculated results for the quasi-static and the dynamic compressive behaviors of the 12% PSMAs (49.1Ni-50.9Ti (at.%)) are compared with the experimental results given by Nemat-Nasser et al.[3] in the present subsection. Table 5 shows the material constants used in the calculations. The material constants are the same for the quasi-static and the dynamic calculations.

The strain rate in the quasi-static calculations is 0.001/s. The calculated and the experimental stress-strain curves are shown in Figs. 6-8. Figure 6 shows the stress-strain relations when the temperature is 23℃ which almost coincides with the temperature for finishing austenite transformation (A_f). In this case, the complete recovery to the austenite phase takes place with no residual strains, exhibiting the perfect superelasticity.

Figure 7 shows the stress-strain relation at 0℃ lower than the temperature for starting austenite transformation (A_s), which is accompanied by a large residual strain after the unloading. There seems to be a mixture of the martensite phase and the austenite phase after the unloading in the experimental results, which is probably due to the experimental error caused by the scattering of the mechanical characteristics of the specimens.

Figure 8 shows the stress-strain relation at -20℃ almost the same as the temperature for starting martensite transformation. In this case, the transformation to the martensite phase starts immediately after the loading, remaining a large residual strain after the unloading. The quasi-static stress-strain curves shown in Figs. 6-8 have totally corresponded well with the experimental results.

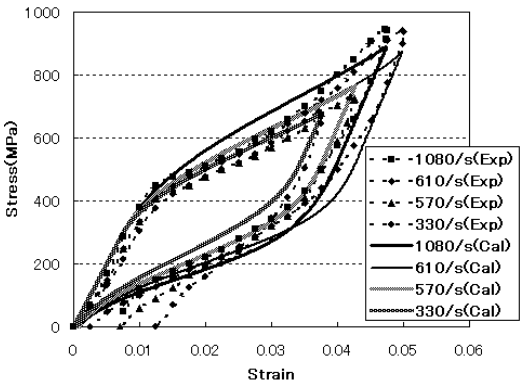

Fig. 5 Dynamic stress-strain curves of dense SMAs at a constant temperature of 23℃ and the indicated strain rates

Table 5 Material constants of 12% porosity SMAs (49.1Ni-50.9Ti (at.%))

Modulus	E_a(MPa)	70000
	E_m(MPa)	30000
	Θ(MPa/℃)	0.55
	C_M(MPa/℃)	4.0
	C_A(MPa/℃)	4.0
	β	0.15
	η (sec)	1.8×10^{-5}
	γ	3.0
Critical stresses	σ_s^{cr}(MPa)	0.0
	σ_f^{cr}(MPa)	500.0
Transformation temperatures	A_s(℃)	1.3
	A_f(℃)	23.8
	M_s(℃)	-20.0
	M_f(℃)	-46.0
Maximum residual strain	ε_L	0.09

The temperature in the dynamic calculations is 23℃ as in the experiments. The calculated stress-strain curves at high strain rates (1040/s, 1300/s) are compared with the experimental results in Fig. 9 and Fig. 10. The superelastic behavior with almost full recovery to the austenite phase and no residual strains can be observed as the temperature is 23℃ almost the same as the temperature for finishing austenite transformation (A_f). Although there is a slight difference between the calculations and the experiments probably due to the difficulty in the high speed deformation tests at exactly constant strain rates, they are totally in good agreement with each other.

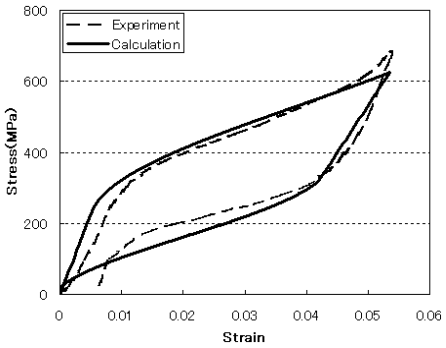

Fig. 6 Quasi-static stress-strain curves of 12% porosity SMAs at a constant temperature of 23℃ and a strain rate of 0.001/s

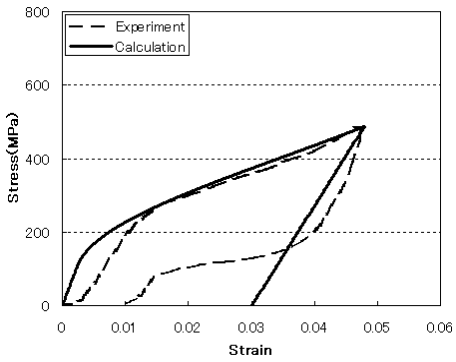

Fig. 7 Quasi-static stress-strain curves of 12% porosity SMAs at a constant temperature of 0℃ and a strain rate of 0.001/s

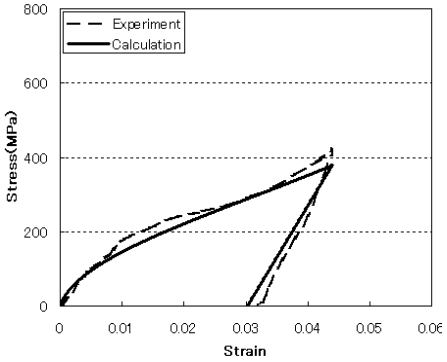

Fig. 8 Quasi-static stress-strain curves of 12% porosity SMAs at a constant temperature of -20℃ and a strain rate of 0.001/s

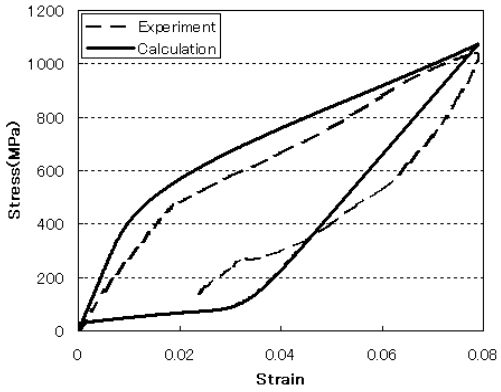

Fig. 9 Dynamic stress-strain curves of 12% porosity SMAs at a constant temperature of 23℃ and a strain rate of 1040/s

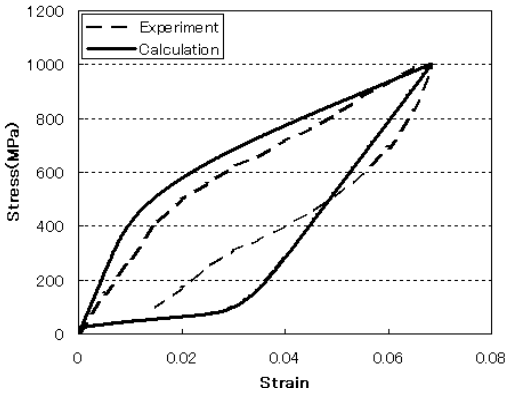

Fig. 10 Dynamic stress-strain curves of 12% porosity SMAs at a constant temperature of 23℃ and a strain rate of 1300/s

3.4 Discussions

The SMAs, which are materially identified in the subsections 3.1, 3.2 and 3.3, are manufactured in a different way with different components, possessing different mechanical characteristics. As a result, they have different material constants as shown in Tables 1-5. Among these material constants, the transformation temperatures in Table 1, Table 5 and the texts as well as the elastic constants in Table 1 and Table 5 are cited from the references[(1),(3),(6)]. The other material constants have been determined so as to fit the constitutive equation proposed in the subsection 2.2 to the experimental results in the literatures.

The present constitutive equation model takes account of the effects of the porosity, the temperature and the strain rate. A good agreement between the present constitutive modeling and the material test results have been confirmed with respect to the porosity in the subsection 3.1, the strain rate in 3.2, and the porosity, the temperature and the strain rate in 3.3. Consequently the validity and the generality of the present constitutive modeling have been illustrated. Furthermore the constitutive models identified in the present study are directly applicable to the finite element analysis of the machine parts and the structures composed of the SMAs or the PSMAs possessing similar mechanical properties.

4. Conclusion

In the present study, the constitutive equation expressed in terms of internal state variables for the quasi-static and dynamic behaviors of the PSMAs have been formulated to predict the mechanical behaviors of the PSMAs considering the strain rate effect. The one-dimensional constitutive equations for the SMAs by the authors[(5)] have been extended to take account of the porosity and the strain rate effect.

The present constitutive modeling has been applied to the simulations of the quasi-static and dynamic, uniaxial compressive behaviors of the PSMAs under the conditions of various strain rates and temperatures. The validity of the proposed constitutive modeling has been illustrated by comparing the calculated results with the experimental results.

The present constitutive equation model is useful as a practical computational model for the prediction of the quasi-static and dynamic behaviors of the PSMAs. The accuracy improvement by the comparison with the experimental results and the applications to the finite element analysis of machine parts and structures are future works.

References

(1) Zhao, Y. et al., Compression Behavior of Porous NiTi Shape Memory Alloy, *Acta Materialia*, Vol. 53 (2005), pp. 337-343.
(2) Lagoudas, D. C. et al., Fabrication, Modeling and Characterization of Porous Shape

Memory Alloys, *Proceedings of SPIE*, Vol.4333 (2001), pp. 141-150.

(3) Nemat-Nasser, S. et al., Experimental Characterization and Micromechanical Modeling of Superelastic Response of a Porous NiTi Shape-Memory Alloy, *Journal of the Mechanics and Physics of Solids*, Vol. 53 (2005), pp. 2320-2346.

(4) Entchev, P. B. and Lagoudas, D. C., Modeling of Transformation-Induced Plasticity and its Effect on the Behavior of Porous Shape Memory Alloys. Part II: Porous SMA Response, *Mechanics of Material*, Vol.36 (2004), pp. 893-913.

(5) Toi, Y. et al., Finite Element Analysis of Superelastic, Large Deformation Behavior of Shape Memory Alloy Helical Springs, *Computers & Structures*, Vol.82 (2004), pp. 1685-1693.

(6) Nemat-Nasser, S. et al., High Strain-Rate, Small Strain Response of a NiTi Shape Memory Alloy, *Journal of Engineering Materials and Technology*, Vol.127 (2005), pp. 83-89.

(7) Auricchio, F. and Taylor, R. L., Shape-Memory Alloys: Modelling and Numerical Simulations of the Finite-Strain Superelastic Behavior, *Computer methods in applied mechanics and engineering*, Vol.143 (1997), pp. 175-194.

(8) Toi, Y. and Kiyosue, T., Three-Dimensional Mesomechanical Analysis of Brittle Solids Containing Microinclusions, *Transactions of the Japan Society of Mechanical Engineers*, Vol. 61, No. 582 (1995), pp. 447-453.

(9) Toi, Y. and Atluri, S.N., Finite Element Analysis of Static and Dynamic Fracture of Brittle Microcracking Solids, Part 1: Formulation and Simple Numerical Examples, *International Journal of Plasticity*, Vol.6 (1990), pp.169-188.

(10) Owen, D. R. J., Hinton, E., *Finite Elements in Plasticity: Theory and Practice*, (1980), p.285, Pineridge Press Limited.